



Effect of the Return-channel Geometric Parameters on the Performance of a Centrifugal Compressor with a High-flow Coefficient

K. Zhao¹, Y. Liu^{1†}, Y. Zhang², Y. Sun², X. Liu², H. Shi²

¹ School of Energy and Power Engineering, Dalian University of Technology, Dalian, Liaoning, 116024, China

² Shenyang Blower Group Co., Ltd, Shenyang, Liaoning, 110869, China

†Corresponding Author Email: yanliu@dlut.edu.cn

ABSTRACT

The return-channel of a preceding stage in a multi-stage centrifugal compressor has a significant effect on the aerodynamic performance of the current and subsequent stages. However, due to the relatively complex nature of the return-channel configuration with many geometric parameters, no general design guidance is available in the literature. In this study, numerical methods are used to study the effects of different geometric parameters of a return-channel on the performance of a high-flow-coefficient centrifugal compressor. A multi-objective genetic algorithm is applied to optimize the return-channel. The effects of different geometric parameters on the performance are then studied using a sensitivity analysis method. Calculation results show that the residual vortex intensity at the outlet of the return-channel is affected by the geometric angles of the inlet and outlet of the return-channel blades. The flow uniformity at the stage outlet is primarily affected by the geometric angle of the blade outlet and the number of blades. The overall performance of the compressor stage is primarily affected by the geometric angle of the blade inlet and the lateral inclination angle of the cover plate. Calculation results for a two-stage compressor consisting of the optimized first stage and its following stage show that the outlet flow field of the first stage is more uniform than the original first stage. Additionally, at the design operating condition, the polytropic efficiency and pressure ratio of the entire unit increase by 1.07% and 4.07%, respectively. The polytropic efficiency and pressure ratio for the second stage increase by 2.34% and 3.51%, respectively. The impeller head coefficient increases by 7.33%. The theoretical analysis shows that for high-flow-coefficient centrifugal compressors, reducing the residual vortex intensity of the outlet flow field of the return-channel in a stage can significantly improve the off-design performance of the following stage.

Article History

Received August 4, 2023

Revised October 12, 2023

Accepted October 29, 2023

Available online January 1, 2024

Keywords:

Return-channel

High flow coefficient

Geometric parameters

Sensitivity analysis

Residual vortex intensity

Multi-objective optimization

1. INTRODUCTION

In the liquefied natural gas and petrochemical industries, high-flow-coefficient ($\varphi > 0.2$) centrifugal compressor stages have significant economic benefits due to their large flow capacities and compact structures [Harvey \(2019\)](#). Therefore, they are commonly used as the first stages of multi-stage centrifugal compressors or the embedded stages of intercooling units. The performance of these stages decisively affects the entire unit.

With the advancement of technology, impeller efficiency has reached an impressive 96% ([Sorokes,](#)

[2013](#)), so making further enhancements is a daunting task. The velocity within the return-channel is notably lower than that in the impeller or the diffuser; thus, under design conditions, the total pressure loss in the return-channel is generally considered to have a relatively minor effect on the overall performance. However, research conducted by [Aalburg et al. \(2011\)](#) revealed that losses within stationary components account for approximately 5–10% of the total unit losses. Furthermore, due to their large radii and flow-path widths, return-channels with high flow coefficients experience more significant internal flow separation and friction losses than do low-flow compressors. In addition, the residual vortices at the return-channel can cause a decrease

NOMENCLATURE			
b	width of passage	θ	title angle
C_p	specific heat coefficient	τ	impeller work coefficient
M_u	machine Mach number	Subscripts	
P_t	total pressure	2	impeller outlet
r	bend radius	4	diffuser outlet
R	radius from the rotation axis	5	return vane inlet
T_t	total temperature	6	return vane outlet
u_2	rotor speed at impeller outer diameter	h	hub
\bar{v}_t	mean circumferential velocity	s	shroud
Δv_t	standard deviation of circumferential velocity	ref	original value
y^+	dimensionless wall distance	U	U-bend
Z	number of vanes	L	L-bend
α	flow angle from meridional direction	Im	impeller
$\bar{\alpha}$	mean flow angle	Dif	diffuser
$\Delta\alpha$	standard deviation of flow angle	Re	return channel
β	vane angle from meridional direction	In	stage inlet
ε	total pressure ratio	Out	stage outlet
η_{pol}	polytropic efficiency	S	small point

in the energy head coefficients of the subsequent impellers, which consequently negatively affect the efficiency and operating range of the entire unit.

Over the past two decades, return-channel research has proliferated significantly. In addition to numerical and empirical investigations of the flow within return-channels (Nakane et al., 1987; Harada, 1988; Veress & Van den Braembussche, 2004; Franz et al., 2015; Xi et al., 2019; Xu et al., 2021), traditional structures have been optimized. Wen et al. (2008) investigated different r/b values for a compressor bend with a flow coefficient of 0.07; they discovered that the bend performance was optimal when this ratio was approximately equal to 1.0. Lenke and Simon (1999) reduced the total pressure loss within a return-channel and enhanced the uniformity of the stage exit flow field by diminishing the outlet width of a compressor bend that had a flow coefficient of 0.12. Reddy et al. (2010) improved the uniformity of the stage exit flow field and mitigated the flow separation on the suction side of a blade by altering the geometric angle of the return-blade inlet in a compressor that had a flow coefficient of 0.053. Hildebrandt and Schilling (2016) studied the blade structure of a return-channel with a flow coefficient of 0.14 and found that the performance of two types of three-dimensional blades was better than that of two-dimensional blades.

In the domain of multi-parameter optimization design, Pazzi et al. (2002) conducted a sensitivity analysis with four geometric parameters of the meridional flow path in a return-channel. They examined the parameter impacts on the losses and the flow field uniformity and used the design of experiments (DOE) methodology to scrutinize the collective effect of multiple parameters on the losses. Hildebrandt (2011) used a genetic algorithm to optimize the blade shape in the return-channel, the U-shaped-bend meridional shape, and the return-channel inlet–outlet width ratio; these optimizations resulted in a total pressure loss reduction of 3%. While maintaining the variable performance of the compressor, Simpson et al. (2008) used the DOE method to investigate the effect of

reducing the expander inlet–outlet radius ratio on a compressor. Nishida et al. (2013) used a genetic-algorithm-based multi-objective optimization method to optimize the geometric parameters of a compressor return-channel when the flow coefficient was 0.105. A sensitivity analysis revealed that the total pressure loss was influenced by the blade inlet–outlet area ratio, that the residual vortex at the outlet was affected by the inlet–outlet radius ratio, and that the number of blades affected both objective functions. Safari et al. (2023) studied the exit width of the return bend, the flow-path inclination, and the diversion blade structure of a return-channel that had a flow coefficient of 0.15; they observed that the use of diversion blades in the return-channel significantly enhanced the overall pressure ratio and the polytropic efficiency.

The optimization design of return-channels predominantly focuses on centrifugal compressors with small and moderate flow rates; there is a conspicuous lack of research regarding compressors with high flow coefficients. Additionally, optimization typically focuses on one or more variables within the return-channel and considers a limited number of design variables; it rarely explores the effects of the variable interactions on the objective functions. Moreover, no studies could be found in the published literature regarding the effects of an optimized return-channel on the subsequent compressor stages.

This study focused on a high-flow centrifugal compressor with a flow coefficient of 0.22. Traditionally, compressors operating at machine Mach numbers exceeding 0.8 and for which the design flow coefficients approach or exceed 0.15 are referred to as high-flow-coefficient compressors. The polytropic efficiency, total pressure ratio, residual vortex intensity (average of the speed and airflow angles), and flow field uniformity (standard deviation of the speed and airflow angles) were taken as objective functions. A sensitivity analysis was conducted with nine critical geometric parameters of the

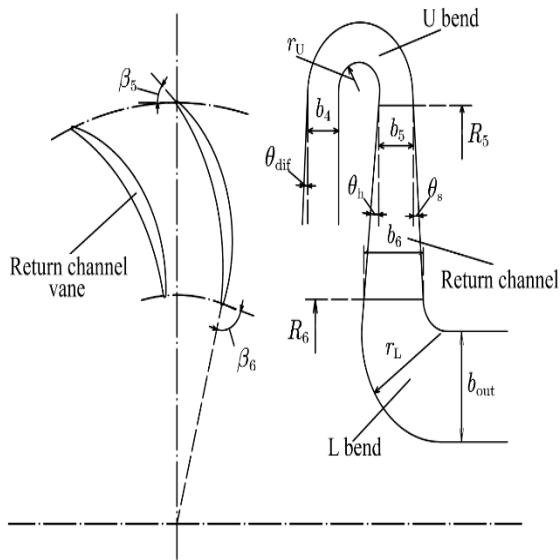


Fig. 1 Return-channel parameters

Table 1 Geometric parameters of the centrifugal compressor investigated during this study

Parameter	Symbol	Value
Number of impeller vanes	Z_{im}	15
Number of return-channel vanes	Z_{re}	18
Outlet-to-inlet radius ratio of the return-channel vane	R_6/R_5	0.50
Outlet-to-inlet width ratio of the U-bend	b_5/b_4	1.10
Hub-side radius ratio of the U-bend	r_U/b_4	0.67
Hub-side radius ratio of the L-bend	r_L/b_{out}	0.98
Hub-side tilt angle of the return-channel	θ_h	6°
Shroud-side tilt angle of the return-channel	θ_s	0°
Geometric angle of the return-channel vane inlet	β_5	40°
Geometric angle of the return-channel vane outlet	β_6	90°

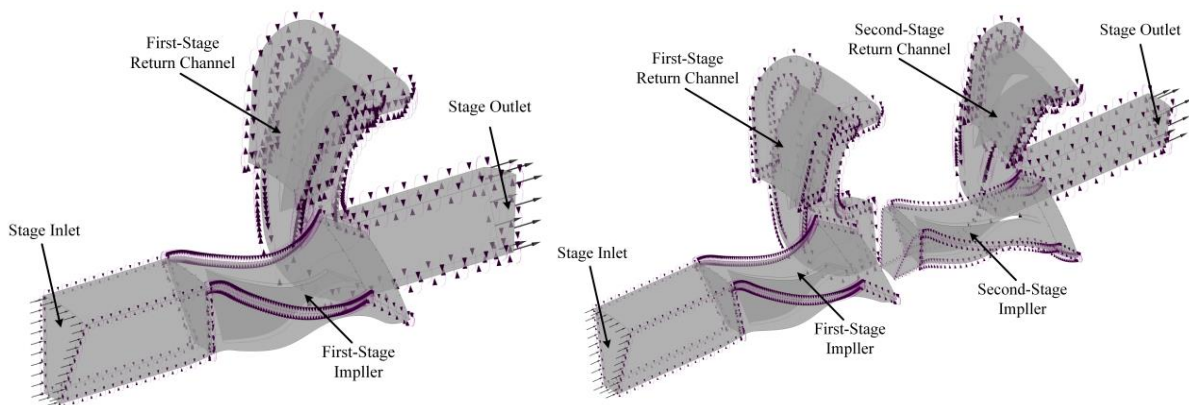
return-channel, and then optimization design was performed using a genetic-algorithm-based multi-objective optimization method. Concurrently, a compressor with a flow coefficient of 0.155 was selected for the second stage, then two-stage numerical calculations were performed for the return-channel both before and after optimization, and the results were subsequently analyzed.

Figure 1 shows the structural schematic and corresponding symbols of the return-channel flow path. It encompassed a U-shaped bend, a return-channel with blades, and an L-shaped bend. The primary geometric parameters are listed in Table 1.

2. Numerical Method

The numerical calculations in this study were performed using the commercial software ANSYS CFX, and the SST model was selected as the turbulence model. The boundary conditions for the centrifugal compressor stage were primarily chosen based on experimental parameters. The boundary at the compressor stage entrance was set as an axially uniform boundary, with total temperature (293 K) and total pressure values (98,000 Pa) specified based on experimental measurements. A mass flow rate boundary condition was specified for the outlet. All the wall surfaces were assumed to be adiabatic and smooth, and no-slip settings were applied. The circumferential boundaries of each component of the compressor stage were given rotating periodic boundary conditions, and the interfaces between the moving and stationary parts used the stage-average model (mixing plane). The working medium was chosen to be air modeled as an ideal gas. Figure 2(a) depicts the computational domain used for numerical accuracy verification and the return-channel design optimization; it consisted of a mixed-flow impeller, a vaneless diffuser, and a return-channel.

The computational domain was grid-partitioned using the Autogrid-5 module in the commercial NUMECA software. High-quality structured grids were generated by adjusting the number of grid nodes, and the grids for the impeller and return-channel are depicted in Fig. 3. To ensure sufficient grid resolution near the wall surfaces and



(a) Calculation domain used in optimization

(b) Calculation domain used in integrated analysis

Fig. 2 Calculation domains

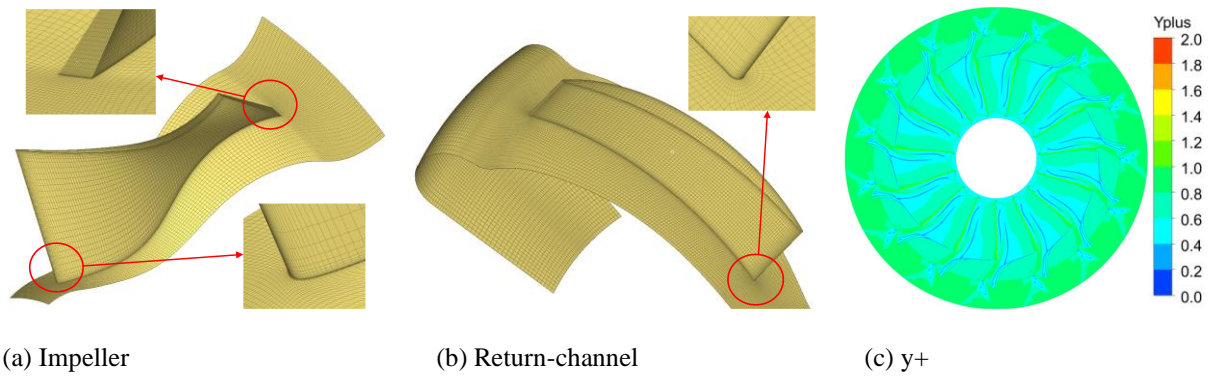


Fig. 3 Single-channel grids for the centrifugal compressor

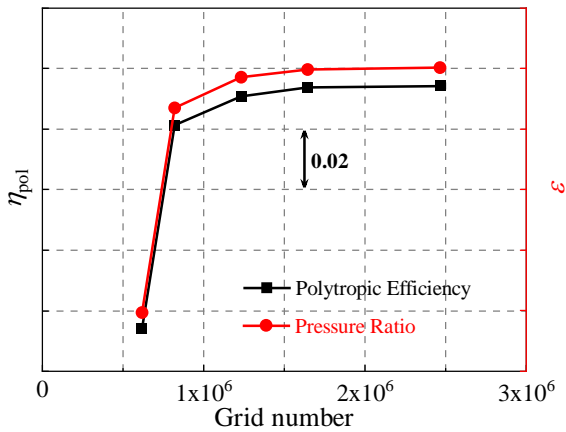


Fig. 4 Mesh independence verification results

near the boundary layers of the impeller blades and the return-channel, the grids near the wall surfaces and within the blades of each component were refined to meet the requirements of the chosen turbulence model. Consequently, the grid height of the first layer near the wall surfaces was set to 1×10^{-6} m, and the overall value of y^+ for the near-wall surfaces of the impeller was kept below 2, as illustrated in Fig. 3(c).

To further ensure the precision of the numerical simulations, a mesh independence verification was conducted for the impeller and the return-channel under the design conditions, as illustrated in Fig. 4. Results were

gathered for five different grid structures; it was apparent that when the number of grid nodes reached approximately 1.64 million, both the pressure ratio and the efficiency ceased to change with the number of nodes. Therefore, by adjusting the topology method of the network and the number of nodes, the total number of grid nodes is kept constant. The sampling check was performed at the sampling points and the result is unchanged. The total pressure ratio and polytropic efficiency definitions can be expressed by Eq. (1) and Eq. (2), respectively:

$$\varepsilon = P_{t,Out} / P_{t,In} \quad (1)$$

$$\eta_{pol} = \frac{\kappa - 1}{\kappa} \ln \left(\frac{P_{t,Out}}{P_{t,In}} \right) / \ln \left(\frac{T_{t,Out}}{T_{t,In}} \right) \quad (2)$$

In Eq. (1) and Eq. (2), κ represents the adiabatic index, which was equal to 1.4 in this study. $P_{t,In}$, $P_{t,Out}$, $T_{t,In}$, and $T_{t,Out}$ represent the average total pressure at the inlet, the average total pressure at the outlet, the total temperature at the inlet, and the total temperature at the outlet, respectively, of the mass flow controller in the compressor stage.

Testing of the variable-speed performance of the centrifugal compressor was conducted on the model test bench of the Shenyang Blower Group Co., Ltd. The test bench configuration and physical representation are depicted in Fig. 5. For more details regarding the measurement apparatus, instrument precision, and data

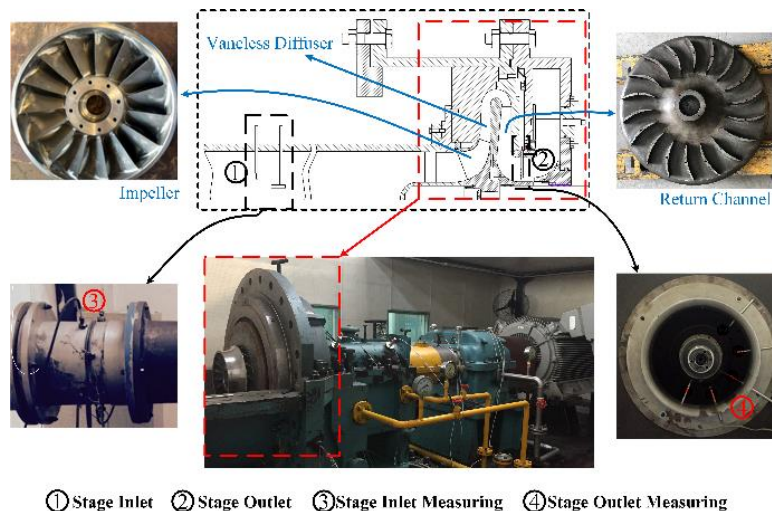
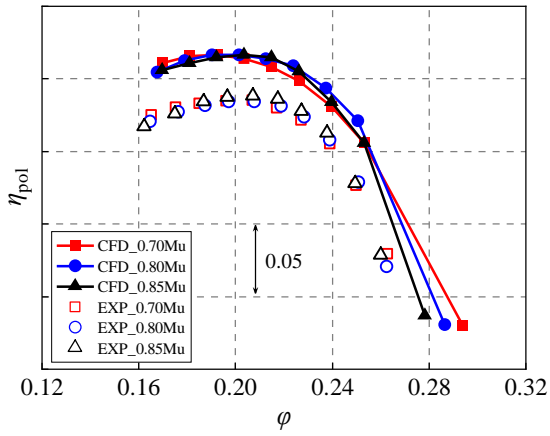
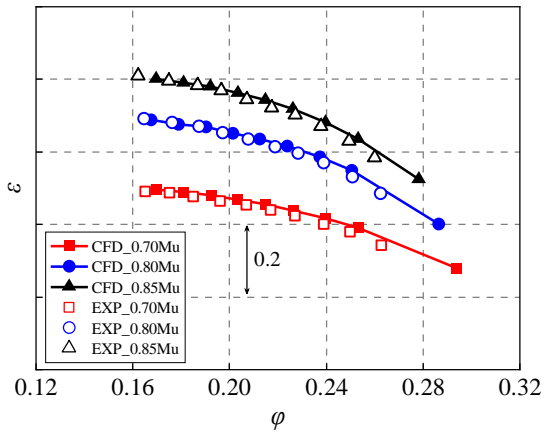


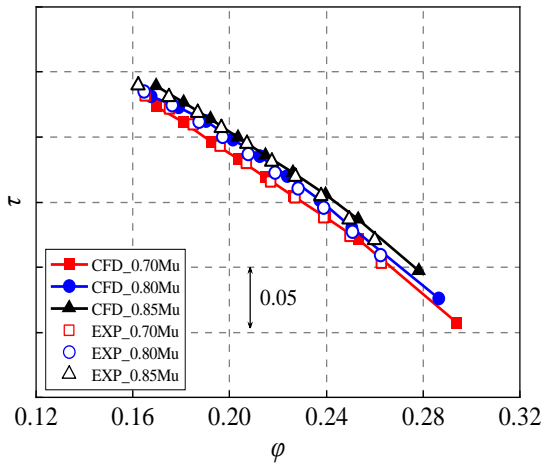
Fig. 5 Test bench



(a) Stage efficiency



(b) Stage pressure ratio



(c) Head coefficient

Fig. 6 Comparison between the experimental and numerical results

acquisition system methodologies, one may refer to the prior work (Zhao et al., 2017; Li et al., 2021). To verify the accuracy of the numerical simulations, a comparison was made between the numerical results and experimentally measured data. Figure 6 presents the aerodynamic performance curves for the compressor when the machine Mach number (Mu) had values of 0.7, 0.8, and 0.85. The definition of Mu is the circumferential velocity at the impeller outlet (u_2) to the velocity of sound

at the impeller inlet (a). The target functions of the ordinate in the figure underwent dimensionless treatment.

Figure 6 shows that the numerically computed aerodynamic performance of the compressor stage aligned reasonably well with the experimental measurements, though there were some residual disparities. The energy coefficient is expressed by Equation (3). Both the calculated overall polytropic efficiency and the pressure ratio exceeded the experimentally measured values, while the energy coefficient values for the impeller were largely consistent. One source of the variance was attributed to the method used to manufacture the impeller, which combined machining and welding. It resulted in reduced precision and significant beveling, thereby causing diminished experimental efficiency. Conversely, the numerical calculations did not consider the beveling at the blade root and tip, the leakage through the disk-cover-side clearance, or the effect of the surface roughness on the results; these all contributed to overestimations of the polytropic efficiency and pressure ratio by the numerical simulations. In a holistic view, the discrepancy between the numerical calculations and the experimental measurements was consistently less than 4%, and the trends aligned, indicating that the adopted numerical simulation methodology was reliable (Weber et al., 2016). It could therefore be used for further optimization studies involving the centrifugal compressor recirculation

$$\tau = \frac{C_p \Delta T}{u_2^2} \quad (3)$$

3. OPTIMIZED RETURN-CHANNEL DESIGN

3.1 Objective Function and Design Variables

In this investigation, Latin hypercube sampling (LHS), the multi-objective genetic algorithm (MOGA), and the Kriging model were used to optimize the design of the return-blades and the meridional contour in the return-channel. The goal of the optimization was to redesign the return-channel shape to maximize the overall stage efficiency and the pressure ratio while minimizing flow non-uniformity at the stage outlet section and reducing residual turbulence. To achieve this outcome, several parameters were selected as objective functions: the polytropic efficiency (η_{pol}) and the pressure ratio (ϵ) of the entire stage, the average meridional airflow angle ($\bar{\alpha}$) at the return-channel outlet, the average tangential velocity (\bar{v}_t) at the return-channel outlet, the standard deviation of the airflow angle ($\Delta\alpha$) at the return-channel outlet, and the standard deviation of the tangential velocity (Δv_t) at the return-channel outlet.

The magnitude of the residual vortex intensity is denoted by $\bar{\alpha}$ and \bar{v}_t , while $\Delta\alpha$ and Δv_t signify the uniformity of the flow (Nishida et al., 2013). Their calculation methods are shown in the following equations:

$$\bar{\alpha} = \frac{\sum m_i \alpha_i}{m}, \quad \bar{v}_t = \frac{\sum m_i v_{t,i}}{m} \quad (4)$$

$$\Delta\alpha = \sqrt{\frac{\sum m_i (\alpha_i - \bar{\alpha})^2}{m}}, \quad \Delta v_i = \sqrt{\frac{\sum m_i (v_{i,i} - \bar{v}_i)^2}{m}} \quad (5)$$

where i represents the nodes in the calculation cross-section, m_i denotes the mass of each node, and m corresponds to the mass of the entire cross-section. Subsequently, a MOGA was used to identify the optimal values of the objective functions.

During the return-channel optimization process, several parameters, such as the exit width (b_4), the exit radius (R_4), the shroud-side tilt angle of the diffuser (θ_{Dif}), the inlet radius of the return-channel vane (R_5), and the exit width of the L-bend (b_{Out}), remained constant. The design variables included the hub curvature radius ratio of the U-bend (r_U/b_4), the outlet-to-inlet width ratio of the U-bend (b_5/b_4), the tilt angles on the hub and shroud sides of the return-channel vane (θ_h and θ_s , respectively), the outlet-to-inlet radius ratio of the return-channel vane (R_6/R_5), the hub-side curvature radius ratio of the L-bend (r_L/b_{Out}), the number of return-channel vanes (Z_{Re}), the geometric angle of the return-channel vane inlet (β_5), and the geometric angle of the return-channel vane outlet (β_6). The value ranges of the design parameter values are shown in Table 2:

The meridional contour on the shroud side of the U-shaped bend was composed of a single circular arc, which could be determined after establishing r_U/b_4 and b_5/b_4 , as well as θ_h and θ_s , which are adjacent and tangential to the shroud side of the bladeless expander and the return flow device, respectively. The meridional contour of the return-flow channel was constructed from circular arcs and straight lines with transition points connected in a tangential manner. The return-channel vane had a simple double-circular-arc structure, where both the shroud and hub sides of the return-flow device were straight lines. Regarding the U-shaped bend, the meridional contour on the shroud side of the L-shaped bend was a single circular arc.

3.2 Optimization Processes

Figure 7 presents a process diagram of the return-channel optimization system. The design objective for this system was to ascertain the optimal return-channel shape, thereby achieving the optimal values for all the objective functions. Within this system, the LHS method was initially used to obtain 100 sets of initial design points from the defined design-variable ranges. Subsequently, computational fluid dynamics (CFD) was used to calculate the objective function values of all the initial design points. The Kriging model was used to establish the functional relationship between 9 input variables and 6 output variables. Then 100 iterations were performed using MOGA. Due to some errors in the Kriging model itself, the selection could not be completely based on the model. Based on this, we selected 3 groups of best examples for numerical calculation and one group for analysis. Upon completion of the optimization process, an

Table 2 Optimization parameters and value ranges

Optimization parameter	Symbol	Value range
Hub-side radius ratio of the U-bend	r_U/b_4	0.5-1.2
Outlet-to-inlet width ratio of the U-bend	b_5/b_4	0.7-1.3
Tilt angles on the hub and shroud sides of the return-channel vane	θ_h, θ_s	-2° - $+6^\circ$
Outlet-to-inlet radius ratio of the return-channel vane	R_6/R_5	0.5-0.6
Hub-side radius ratio of the L-bend	r_L/b_{Out}	0.7-1.1
Number of return-channel vanes	Z_{Re}	15-24
Geometric angle of the return-channel vane inlet	β_5	25° - 55°
Geometric angle of the return-channel vane outlet	β_6	85° - 95°

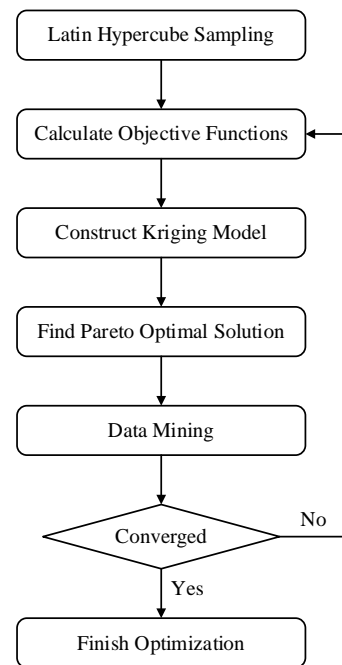


Fig. 7 Flowchart of the optimization system

analysis was conducted of the procured Pareto optimal solutions, and candidate designs were manually selected. These candidate designs were then used in further CFD simulations, and these results were appended to the database. This entire process was performed iteratively until the changes in the Pareto optimal solutions diminished.

3.3 Results and Analysis

Figure 8 exhibits the results of a sensitivity analysis involving nine design variables and six objective functions, wherein the contributions of the individual variables and the mutual interactions between variables are presented as percentages. The six variables with the highest contributions were selected and ranked accordingly, while the cumulative contributions of the remaining design variables were denoted as “others.”

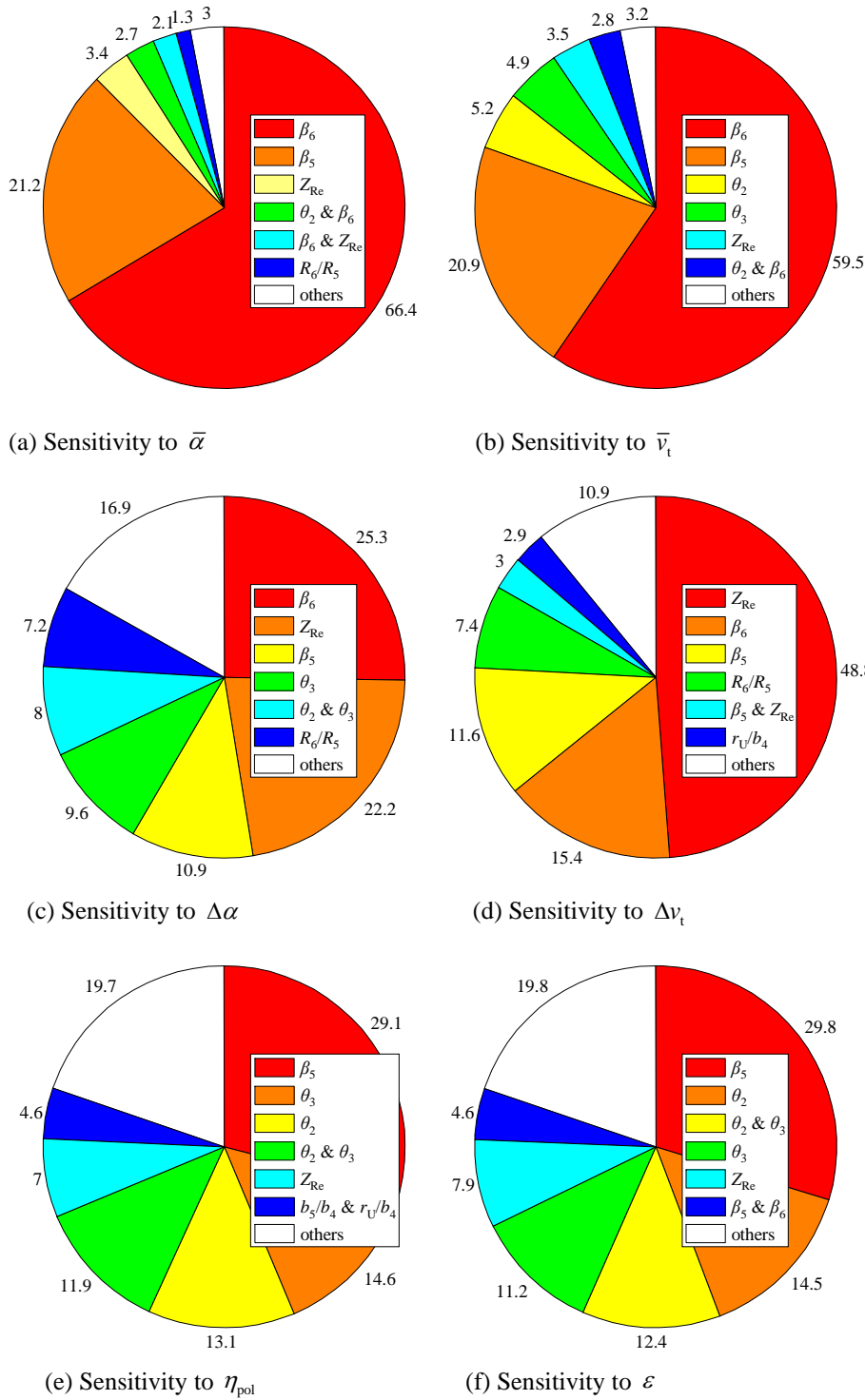


Fig. 8 Sensitivity analysis results

The sensitivity analysis results for the mean airflow angle, $\bar{\alpha}$, and the mean tangential velocity, \bar{v}_t , at the return-channel stage outlet are depicted in Fig. 8(a) and 8(b), respectively. Among all design variables, the geometric angle of the return-channel vane outlet, β_6 , had the most significant effect on these two objective functions, thus demonstrating a clear predominance. However, Nishida et al. (2013) found in the sensitivity analysis of the compressor return-channel with a flow coefficient of 0.105 that the most important factor was the inlet-to-outlet radius ratio of the return vane. It can be seen

that the geometric parameters of the return-channel of the high-flow compressor and the low-flow compressor have different effects on the performance.

Figure 9(a) and 9(b) illustrates the correlations between β_6 and $\bar{\alpha}$ and between β_6 and \bar{v}_t , respectively; the red dotted lines represent the cubic-polynomial fit lines derived from 100 samples of the objective function. These results suggest that within the selected design-variable ranges, as the geometric angle of the blade outlet increases, the absolute values of the mean airflow angle and the tangential velocity at the regenerator

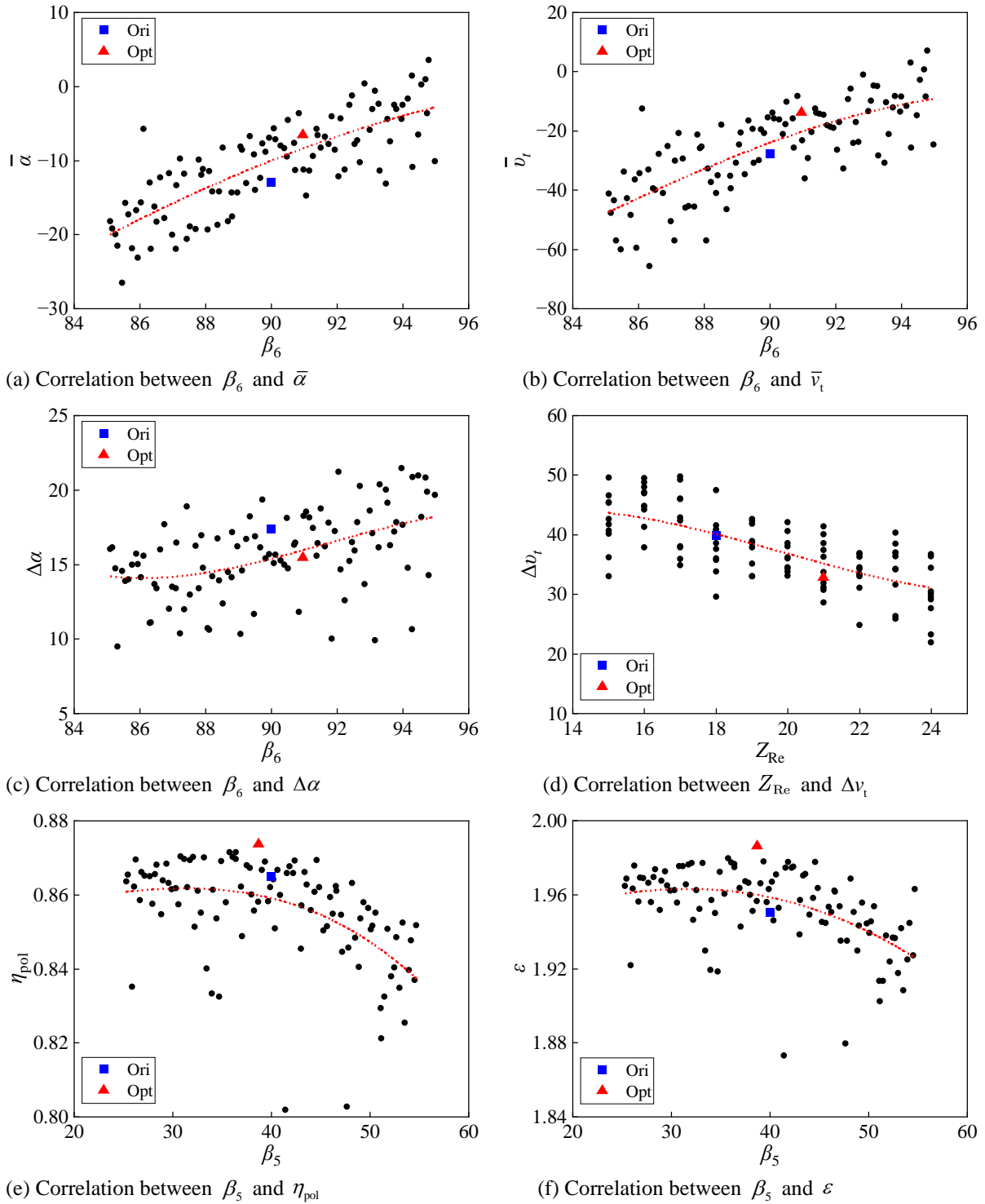


Fig. 9 Relationships between the primary design variables and the objective functions

stage outlet gradually decrease and approach zero, exhibiting linear relationships overall. Therefore, to achieve superior mean airflow angle and tangential velocity values at the return-channel stage outlet, it would be prudent to moderately increase the geometric angle of the return-channel vane outlet.

The sensitivity analysis results for the standard deviation of the airflow angle at the stage outlet, $\Delta\alpha$, as depicted in Fig. 8(c), reveal no absolute dominant design variable. The primary design variable, β_6 , accounted for 25.3% of the total sensitivity, while the secondary design

variable, which was the number of regenerator blades, Z_{Re} , represented 22.2%. The values for these two variables were similar and together they approached 50%. Therefore, an analysis of the correlations between these two design variables and the objective function was warranted.

Figure 9(c) exhibits the correlation between $\Delta\alpha$ and the primary design variable, β_6 . This pattern is consistent with the relationships between $\bar{\alpha}$ and β_6 ; all the patterns show increases in the objective function with increases in

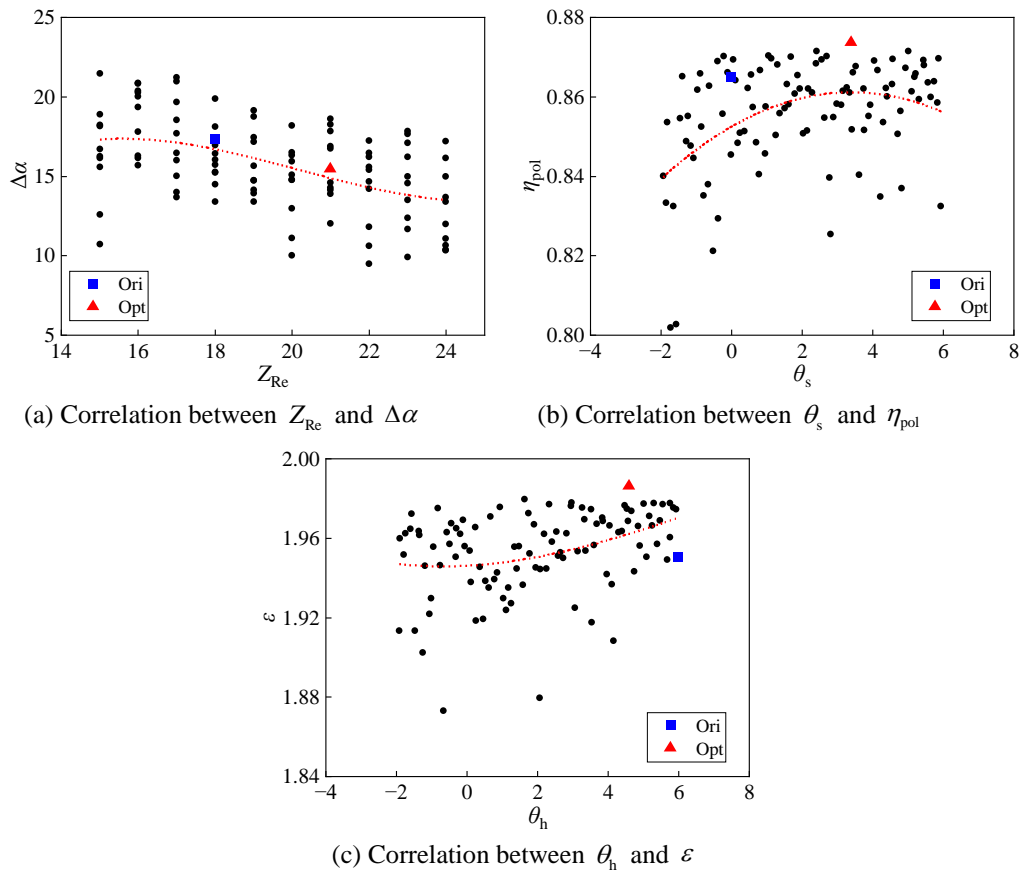


Fig. 10 Relationships between the secondary design variables and the objective functions

the primary design variable. However, because the standard deviation represents the degree of variation in a design variable, a smaller value is desirable; therefore, to achieve a better standard deviation for the airflow angle, the value of the primary design variable should be reduced. This, however, contradicts the previously mentioned perspective that increasing the primary design variable could effectively guide the airflow deflection. An increase in the primary design variable could cause the airflow deflection to be guided more effectively by reducing the mean airflow angle at the stage outlet after passing through the L-shaped bend. However, excessive deflection could cause a large flow-separation region on the suction side of the blade, thereby increasing the turbulence in the flow field at the stage outlet. Therefore, a judicious selection of the value of the primary design variable is required to achieve better standard deviation values for the outlet airflow angle, the mean airflow angle at the stage outlet, and the tangential velocity.

It is evident from Figure 8(d) that the number of blades in the return-channel holds an unequivocal influential position in the sensitivity analysis results for the standard deviation of the tangential speed at the stage outlet, Δv_t . A distinct correlation is also displayed in Fig. 9(d). As the number of blades increases, Δv_t correspondingly decreases, which is consistent with the correlation between the standard deviation of the flow angle and the number of blades of its secondary design variable, as shown in Fig. 10(a). The subject of this study was a high-flow centrifugal compressor with a flow coefficient of 0.22 that was predominantly characterized

by its large channel width. The blade passage of this type of compressor is more prone to flow separation than that of a small-flow compressor, so the flow losses within its stationary components are enhanced, and the non-uniformity of the flow field at the stage outlet is intensified. These both impair the performance of downstream stages. Consequently, it is imperative to appropriately increase the number of blades to guide the flow. This is also why the number of return-channel vanes is the secondary influencing factor of $\Delta\alpha$.

The sensitivity analysis results for the overall stage variable efficiency, η_{pol} , and the pressure ratio, ε , are depicted in Fig. 8(e) and 8(f), respectively. The plots show that the nine design variables were unable to exert decisive effects. These results are similar to those for $\Delta\alpha$. The primary design variable for both of these objective functions was the geometric angle of the blade inlet, β_5 , while the top three secondary design variables were the tilt angles of the hub and shroud sides of the return-channel and their interaction. The proportion of the top four variables was similarly significant. It can thus be inferred that the geometric angle of the return-channel vane inlet and the tilt angle of the return-channel on both sides of the casing are important factors that influence the overall stage efficiency and the pressure ratio.

Figure 9(e) and 9(f), respectively, illustrates the correlations between β_5 and η_{pol} and between β_5 and ε . The figure shows that as β_5 increases, the efficiency and pressure ratio both remain constant initially and then

Table 3 Design variables and objective functions of the original and optimized designs

Design variables	Ori	Opt	Objective functions	Ori	Opt
θ_h	6.00	4.61	η_{pol}	86.49%	87.36%
θ_s	0.00	3.39	ε	1.9503	1.9862
β_5	40.00	38.72	$\bar{\alpha}$	-12.92	-6.57
β_6	90.00	90.91	\bar{v}_t	-27.84	-13.91
Z_{Re}	18	21	$\Delta\alpha$	17.33	15.43
r_U/b_4	0.67	0.84	Δv_t	39.1	32.72
b_5/b_4	1.10	0.99			
R_6/R_5	0.50	0.54			
r_L/b_{out}	0.98	0.91			

decrease. Therefore, it is recommended that the initial geometric angle should be slightly less than 40° . Figure 10(b) shows the correlation between η_{pol} and its secondary influencing factor, θ_s . As θ_s increases, η_{pol} initially increases and then decreases; therefore, it is suggested that the value of θ_s should be between 2° and 5° . Figure 10(c) depicts the correlation between ε and its secondary influencing factor, θ_h . The two are positively and linearly correlated, but an excessive value of θ_h will cause the hub side of the return-channel to be too near the impeller of this stage, thereby affecting the impeller installation. Therefore, the value of θ_h should not exceed 6° .

Five of nine design variables were identified in the preceding discussion. The remaining four have minor effects on the objective functions, so they are not elaborated upon in this paper. The selection of candidate solutions from the previously mentioned 100 examples was dependent upon the enhancement of all six objective functions, and the Pareto optimal solution method was used to derive the ultimate optimization scheme (referred to as Opt). Table 3 compares the design variables and objective functions of both the original scheme (referred to as Ori) and Opt. It reveals significant increases in the η_{pol} and ε objective functions, while the residual vortex strength ($\bar{\alpha}$, \bar{v}_t), which is indicative of the quality of the outlet flow field, decreases by half. The homogeneity ($\Delta\alpha$, Δv_t), however, increased only marginally, implying that the residual vortex strength had a primary effect on the performance. Figure 11 depicts a comparison of the meridional contour and blade shape of the return-channel before and after optimization using the primary design variables denoted in Figs 9 and 10.

Figure 11 illustrates that the optimized structure possesses more blades than the original structure, thereby enhancing the airflow guidance and mitigating the flow separation on the suction side of the return-channel. Additionally, with the augmentation of the return-channel cover-side tilt angle and the reduction in the width of the return-blade inlet, the expansion ratio of the return-channel experienced an increase of approximately 16.88%; this further decreased the flow speed within the channel and yielded a more uniform flow field at the stage outlet. As indicated in Table 3, all the objective functions

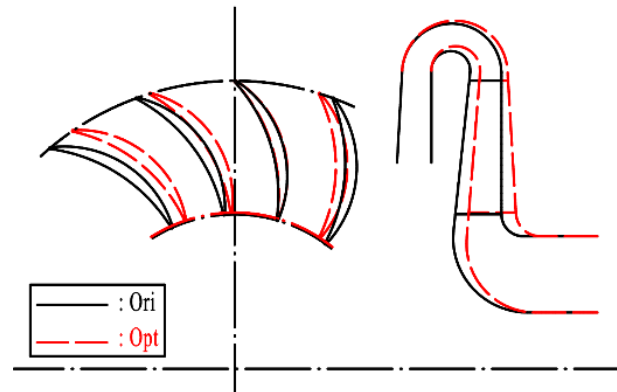


Fig. 11 Blade and meridional shapes of the return-channel in the original and optimized designs

of the optimized structure were superior to those of the original structure. These computational outcomes denote that this optimization methodology is conducive to better airflow guidance within the return-channel, augmenting the performance of the entire stage and providing a more uniform inlet flow field for the downstream impeller.

3.4 Performance Comparison

To assess the effect of the optimized return-channel on the subsequent compressor stages, a compressor with a flow coefficient of 0.155 was used during this study as the second stage in two-stage calculations. The exit diameter of the impeller in the second stage was equal to that in the first stage, 0.4 m. The computational domain for the two-stage calculations was composed of two impellers and two return-channels, as illustrated in Fig. 2(b). A similar grid-partitioning approach was applied to this domain, resulting in a total of approximately 3.41 million grid cells.

Figure 12 shows variable operating performance curves for the first stage of the two-stage calculations. Curves for both the original and optimized designs are displayed. The diagram shows that the energy coefficient of the impeller remained essentially constant after optimization, while the polytropic efficiency and pressure ratio of the entire stage exhibited significant improvements of 0.53% and 0.37% at the design point, respectively, after optimization. Given that the geometric structure of the impeller remained unchanged, the performance enhancement was conspicuous. This suggests

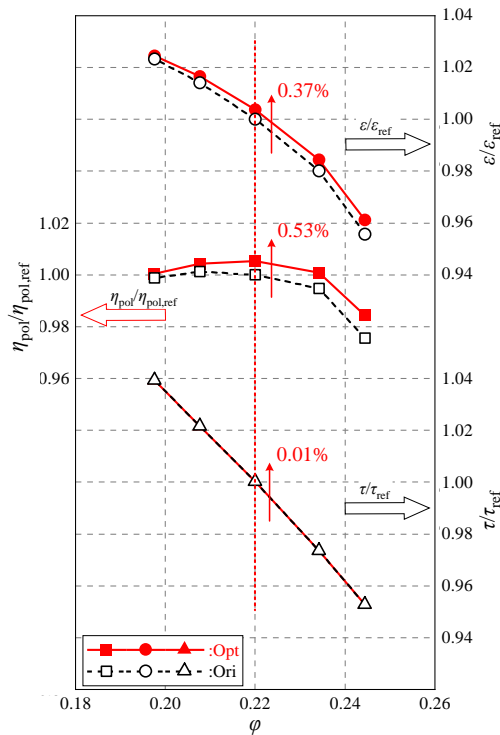


Fig. 12 First-stage performance characteristics

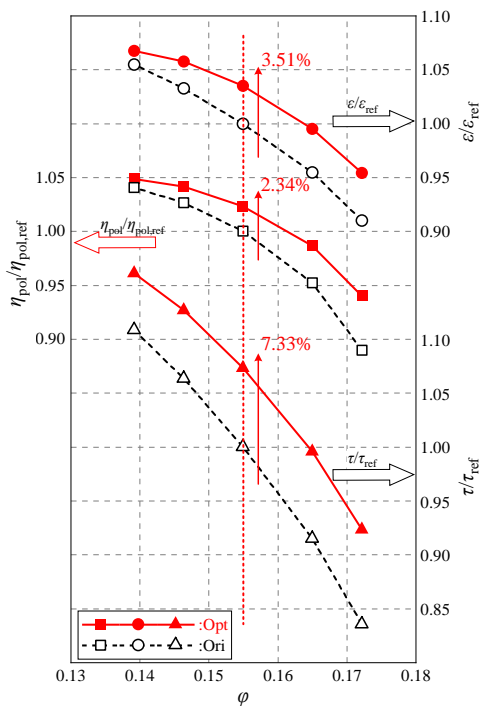


Fig. 13 Second-stage performance characteristics

that even when the impeller performance has plateaued, the return-channel performance still has substantial room for improvement. A comparison of the efficiency and pressure ratio curves before and after optimization indicates that the performance improved most noticeably under high-flow conditions, while the increases were less pronounced under low-flow conditions. This result indicates that the expansion-degree distribution pattern of the optimized return-channel and the increased number

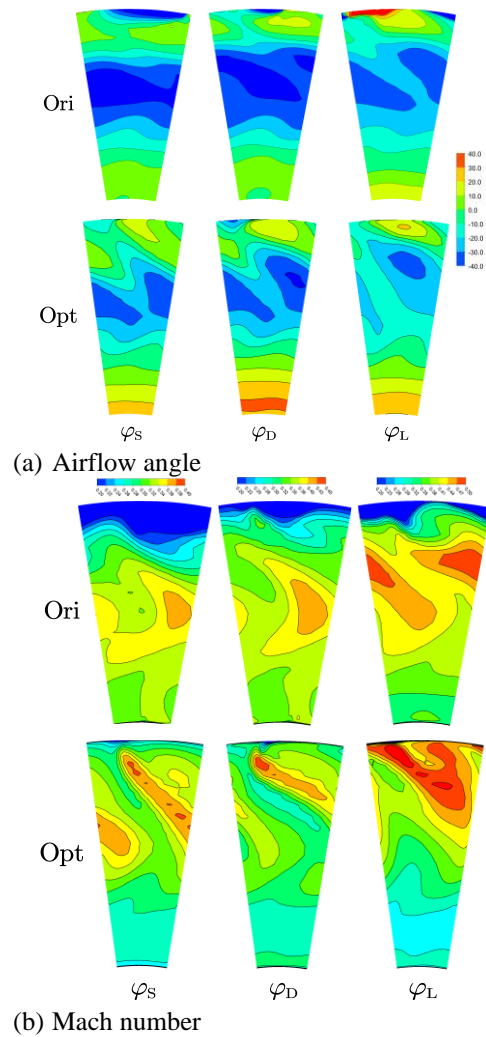


Fig. 14 Outlet airflow angle and Mach number distributions for the first-stage return-channel

of blades have greater airflow-deflection guidance and flow-separation reduction effects under high-flow conditions.

Figure 13 exhibits the variable operating performance curves for the compressor with a flow coefficient of 0.155 resulting from the two-stage calculations. The diagram reveals that all three objective functions increased substantially as a result of the optimization. Additionally, the improvement trends for the efficiency and pressure ratio correspond to those in Fig. 12; the greatest improvements for this second stage also occurred under high-flow conditions. At the design conditions, the energy coefficient, efficiency, and pressure ratio of the second-stage impeller increased by 7.33%, 2.34%, and 3.51%, respectively.

It is evident from the comparative analysis above that the substantial enhancements in the second-stage performance were consequences of the improvements in the first-stage return-channel performance. A comparison of the variable-operating-condition airflow angles and Mach number distributions at the exit of the first-stage return-channel is illustrated in Fig. 14.

As can be seen from the comparison diagram of the flow angle distribution in Fig. 14 (a), the optimized flow

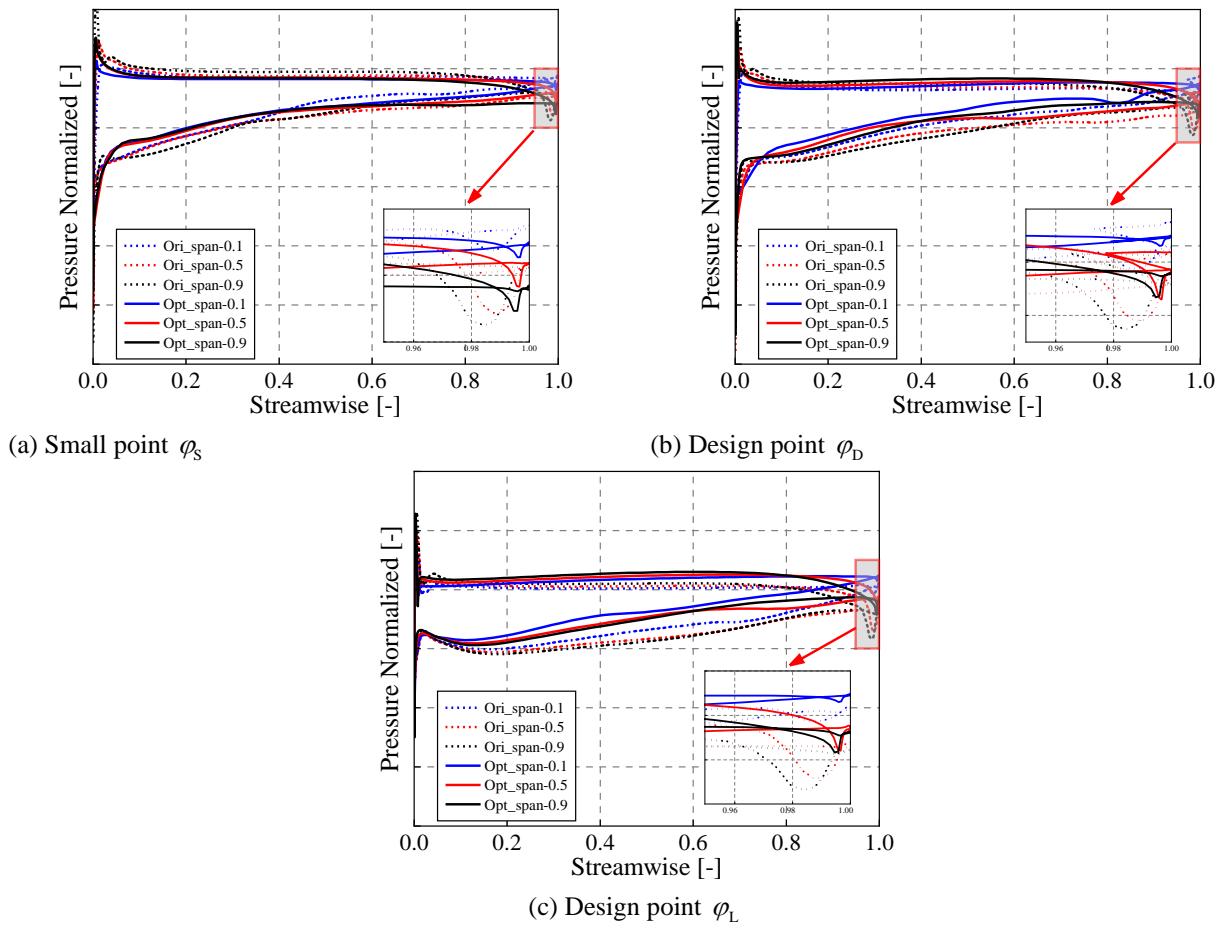


Fig. 15 Static pressure loading distributions of the first-stage return-channel blade

angle distribution is more uniform in the three working conditions, and the negative flow angle area (blue area in Fig. 14) is significantly weakened. At the same time, in the optimized flow angle distribution, the obvious periodic change in the centre of the flow channel can be seen.

As can be seen from the comparison diagram of Mach number distribution in Fig. 14 (b), the flow at the outlet of the optimized return-channel migrates towards the cover side, eliminating the flow separation area at the cover side of the original structure. However, at high flow rates, the increase in flow rate is too large and the performance improvement is not the same as the flow angle distribution in the case. Overall, the optimized return-channel improves the flow at the outlet of the stage and provides a better inlet condition for the next stage.

The sensitivity analysis results discussed in Section 3.3 indicate that the factor with the largest effect on the return-channel outlet flow field is the geometric angle of the blade outlet. By increasing the geometric angle of the blade outlet in compressors with high flow coefficients, it is possible to diminish the intensity of the outlet residual vortex ($\bar{\alpha}$, \bar{v}_t). The static pressure distributions of the return-channel blade, shown in Fig. 15, reveal that the static pressure distribution patterns at three spanwise heights (span-0.1, span-0.5, and span-0.9) were essentially the same over 95% of the blade length before and after optimization. However, there were noticeable differences near the exit, at which point the static pressure of the original structure decreased significantly, which is a clear

indication of flow separation. The increased geometric angle of the blade outlet in the optimized structure reduced the flow-separation intensity and region at the trailing edge of the blade, thereby diminishing the intensity of the residual vortex in the outlet flow field.

The spanwise distributions of the airflow angle and tangential velocity at the first stage outlet for different operating conditions are shown in Fig. 16. The figure shows that the flow directions at the hub and shroud sides are opposite to those at the centre of the passage, which is consistent with previous studies (Jariwala et al., 2016). A comparison of the results for the original and optimized structures shows that the airflow angle and tangential velocity distribution at the shroud side were essentially the same for both, but both shifted to the right below 80% of the blade height after optimization. However, the changes in uniformity were not significant, as shown in particular in Table 2. This means that the performance improvement of the second stage of the compressor was not primarily due to the uniformity of the flow field at the outlet of the return channel.

Figure 17 presents overall performance curves for the entire unit, that is, the two-stage compressor. The figure shows that, for the design conditions, the overall efficiency and pressure ratio increased by 1.07% and 4.07%, respectively, because of the optimization. As inferred from the analysis discussed previously, the structural optimization of the first-stage return-channel initially enhanced the return-channel performance while

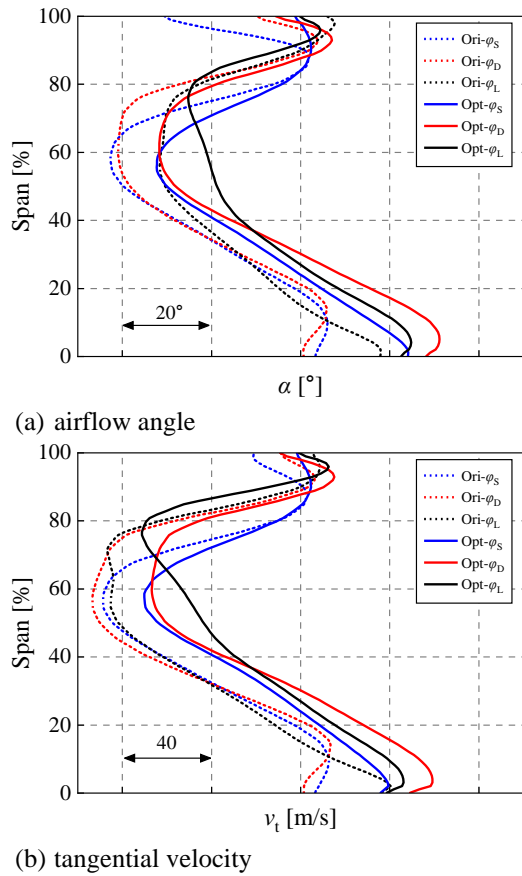


Fig. 16 Spanwise distributions of the airflow angle and tangential velocity at the first-stage outlet

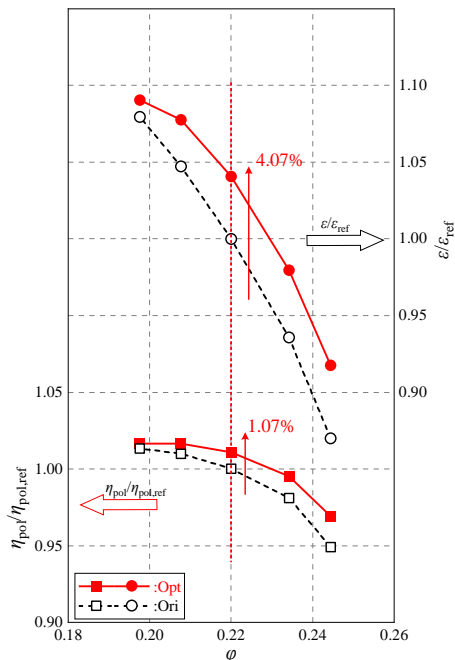


Fig. 17 Overall performance characteristics

simultaneously producing a smaller residual vortex intensity in the axial inlet flow field for the next stage. This resulted in a substantial enhancement in the performance of the second stage as well as that of the entire unit.

4. CONCLUSIONS

Effects of the geometric shape of the return-channel of a high-flow-coefficient centrifugal compressor on the performance have been numerically investigated in this work. A multi-objective optimization method based on a genetic algorithm has been used to optimize the return-channel in order to improve the performance of the first centrifugal compressor and is following stage. Two main conclusions can be drawn:

1. Sensitivity analysis results indicate that the residual vortex intensity at the return-channel outlet is influenced by the geometric angles of the return-blade inlet and outlet. The flow uniformity is primarily affected by the geometric angle at the return-blade outlet and the number of blades. The performance of the entire stage is primarily influenced by the combined effects of the geometric angle of the return-blade inlet and the tilt angle of the end cover.
2. The predicted results for the two-stage compressor with the optimized return channel investigated show that the overall efficiency and pressure ratio of the first stage increase by 1.07% and 4.07%, respectively. The efficiency, pressure ratio, and energy head coefficient of the second stage are improved by 2.34%, 3.51%, and 7.33% respectively. This is due to reduction in the residual vortex intensity and the improvement of flow uniformity at the outlet of the upstream return-channel.

ACKNOWLEDGEMENTS

The authors are grateful for the support of the Shenyang Blower Group Co., Ltd.

CONFLICT OF INTEREST

The authors have no conflicts to disclose.

AUTHORS CONTRIBUTION

K. Zhao: Conceptualization, Methodology, Validation, Writing-review & editing, Software. **Y. Liu:** Methodology, Writing-review & editing. **Y. Zhang:** Methodology, Writing-review & editing. **Y. Sun:** Methodology, Experimental measurement. **X. Liu:** Experimental measurement. **H. Shi:** Experimental measurement.

REFERENCES

- Aalborg, C., Sezal, I., Haigermoser, C., Simpson, A., Michelassi, V., & Sassanelli, G. (2011). *Annular cascade for radial compressor development*. Turbo Expo: Power for Land, Sea, and Air. <https://doi.org/10.1115/GT2011-46834>
- Franz, H., Rube, C., Wedeking, M., & Jeschke, P. (2015). *Numerical investigation of the return channel of a high-flow centrifugal compressor stage*. Turbo Expo: Power for Land, Sea, and Air. <https://doi.org/10.1115/GT2015-43640>

- Harada, H. (1988). Experimental study on the stage performance of a multistage centrifugal compressor. *Nippon Kikai Gakkai Ronbunshu, B Hen;(Japan)*, 54(498).
<https://www.osti.gov/etdeweb/biblio/7030222>
- Harvey, S. (2019). Balancing the economies of scale. *Hydrocarbon Engineering*, (7), 24.
https://www.nstl.gov.cn/paper_detail.html?id=67d27a8a4e3134d47bd350617d0f8c1e
- Hildebrandt, A. (2011). *Aerodynamic optimisation of a centrifugal compressor return channel and U-turn with genetic algorithms*. Turbo Expo: Power for Land, Sea, and Air. <https://doi.org/10.1115/GT2011-45076>
- Hildebrandt, A., & Schilling, F. (2016). *Numerical and experimental investigation of return channel vane aerodynamics with 2D and 3D vanes*. Turbo Expo: Power for Land, Sea, and Air. <https://doi.org/10.1115/GT2016-57713>
- Jariwala, V., Larosiliere, L., & Hardin, J. (2016). Design exploration of a return channel for multistage centrifugal compressors. *Turbo Expo: Power for Land, Sea, and Air*, <https://doi.org/10.1115/GT2016-57777>
- Lenke, L., & Simon, H. (1999). *Numerical investigations on the optimum design of return channels of multi-stage centrifugal compressors*. Turbo Expo: Power for Land, Sea, and Air. <https://doi.org/10.1115/99-GT-103>
- Li, S., Liu, Y., Li, H., & Omid, M. (2021). Numerical study of the improvement in stability and performance by use of a partial vaned diffuser for a centrifugal compressor stage. *Applied Sciences*, 11(15), 6980.
<https://doi.org/10.3390/app11156980>
- Nakane, I., Ariga, I., Hayata, T., & Uchida, M. (1987). Experimental Investigation on return passage of multi-stage compressor. *JSME-B*, 54(503), 1677-1684.
<https://doi.org/10.1299/kikaib.54.1677>
- Nishida, Y., Kobayashi, H., Nishida, H., & Sugimura, K. (2013). Performance improvement of a return channel in a multistage centrifugal compressor using multiobjective optimization. *Journal of Turbomachinery*, 135(3), 031026.
<https://doi.org/10.1115/1.4007518>
- Pazzi, S., Martelli, F., Michelassi, V., & Giachi, M. (2002). *The use of artificial neural networks for performance prediction of return channels for industrial centrifugal compressors*. Turbo Expo: Power for Land, Sea, and Air. <https://doi.org/10.1115/GT2002-30392>
- Reddy, K. S., GV, R. M., & Dasgupta, A. (2010). Flow investigations in the crossover system of a centrifugal compressor stage. *International Journal of Fluid Machinery and Systems*, 3(1), 11-19.
<https://doi.org/10.5293/IJFMS.2010.3.1.011>
- Safari, M., Anbarsooz, M., & Niazmand, H. (2023). The effects of the return channel geometry on the aerodynamic performance of a centrifugal compressor: A numerical study. *Proceedings of the Institution of Mechanical Engineers, Part A: Journal of Power and Energy*, 09576509231157229.
<https://doi.org/10.1177/09576509231157229>
- Simpson, A., Aalburg, C., Schmitz, M., Pannekeet, R., Larisch, F., & Michelassi, V. (2008). *Design, validation and application of a radial cascade for centrifugal compressors*. Turbo Expo: Power for Land, Sea, and Air. <https://doi.org/10.1115/GT2008-51262>
- Sorokes, J. M. (2013). *Range versus Efficiency-striking the proper balance*. Proceedings of the 42nd Turbomachinery Symposium, <https://doi.org/10.21423/R1BP89>
- Veress, A. R. d., & Van den Braembussche, R. (2004). Inverse design and optimization of a return channel for a multistage centrifugal compressor. *Journal of Fluids Engineering*, 126(5), 799-806.
<https://doi.org/10.1115/1.1792258>
- Weber, A., Morsbach, C., Kügeler, E., Rube, C., & Wedeking, M. (2016). *Flow analysis of a high flowrate centrifugal compressor stage and comparison with test rig data*. Turbo Expo: Power for Land, Sea, and Air. <https://doi.org/10.1115/GT2016-56551>
- Wen, S., Hu, X., Zhang, Y., Wang, J., & Li, T. (2008). Optimal r/b ratio of bend channel in centrifugal compressor. *Frontiers of Energy and Power Engineering in China*, 2, 381-385.
<https://doi.org/10.1007/s11708-008-0084-4>
- Xi, G., Tian, Y., Guo, Y., Tang, Y., & Wang, Z. (2019). *Experimental and numerical investigations on flow losses of a U-Bend and return channel system for centrifugal compressor*. Turbo Expo: Power for Land, Sea, and Air. <https://doi.org/10.1115/GT2019-90559>
- Xu, H., Yang, X. I., Jariwala, V., & Larosiliere, L. (2021). *Comparative aerodynamic assessment of a multistage centrifugal compressor return channel based on rans and les*. AIAA Scitech 2021 Forum. <https://doi.org/10.2514/6.2021-0263>
- Zhao, P. F., Liu, Y., & Wang, X. F. (2017). Analysis of vortices and performance of different diffusers in a large mass flow coefficient centrifugal compressor. *Proceedings of the Institution of Mechanical Engineers, Part A: Journal of Power and Energy*, 231(4), 253-273.
<https://doi.org/10.1177/09576509177013>